

Engineering a Macroscopic Adhesion System Inspired by Mucilaginous Seeds

Ufuk Gürer, Felicitas von Usslar, Cordt Zollfrank, and Oliver Lieleg*

Wet adhesion is a challenging process that requires successful interactions between the two surfaces of interest. Current adhesives may offer sufficient strength but often contain toxic components. Thus, when the field of adhesion meets bioinspiration, there is lots of potential for finding an innovative solution. Here, inspired by mucilaginous seeds and by using refined fiber structures provided by renewable materials, it is demonstrated how to build a comparably strong wet adhesive system. The process involves the controlled fibrillation of a wood surface followed by the application of a macromolecular coating employing the main component found in mucilaginous seeds. Moreover, the additional introduction of a thermo-responsive polymer into the system allows for obtaining control over the strength and the compliance of the detachment process. Thus, this study demonstrates how combining renewable materials with a multi-step coating process offers an environmentally friendly solution that pinpoints a promising path toward bio-based wet adhesives.

a typical example for such a scenario, where materials science is still struggling: Even though there are commercial adhesives that work well under wet conditions, they typically make use of chemicals that can be environmentally toxic such as cyanoacrylate,^[1] epoxy resins,^[2] and polyurethanes.^[3] In contrast, nature provides remarkable examples of wet adhesion systems that are not only efficient but make use of biological and non-toxic components only. Examples include octopus suckers,^[4] the adhesion plates produced by barnacles^[5] and the protein-based byssus used by mussels.^[6]

If two materials are brought into contact with each other with the goal to stick them together, two key factors determine the success and strength of the adhesion system: the topography and the surface chemistry^[7] of the involved

1. Introduction

Sometimes, glues are more efficient than we want them to be – removing a paper sticker from a piece of budget furniture can be an annoying and time-consuming task. Conversely, there are situations where achieving good and stable adhesion remains a significant challenge. The controlled adhesion in wet environments is


materials, and both parameters can be tuned to achieve an optimal interaction of the two surfaces. Also in nature, examples of topographical and chemical contributions to adhesion can be observed: for instance, unique topographical structures are seen in dock beetles^[8] and stick insects,^[9] and dedicated chemical moieties are employed by, for example, mussels and tendrils.^[10] In detail, mussels achieve adhesion through the catechol-type molecule levodopa (L-3,4-dihydroxyphenylalanine),^[11] resulting in long-term bonding in wet environments. However, catechol-based adhesives can lose their adhesive properties in acidic environments.^[12] Tendrils and roots on the other hand adhere to and ascend vertical surfaces by secreting mucilage.^[10,13]

Inspired by those examples found in nature, researchers have set out to combine topographical modifications of a surface with suitable chemical moieties to achieve good wet adhesion.^[14] By mimicking the surface architecture of gecko's feet and subsequently coating it with a mussel-inspired polymer containing dopa, Lee et al.^[15] have successfully developed an adhesive that works well in both, wet and dry conditions. Still, to accomplish wet adhesion, a water insoluble (and therefore non-biodegradable) polymer had to be used – but a fully bio-based system might be favorable. In addition, it is also possible to create surfaces with switchable adhesion properties. Those strategies typically incorporate responsive polymers into the material and then switch the configuration of those responsive polymers by external triggers such as light exposure,^[16] chemical stimuli,^[17] or thermal energy.^[18,19] Among those examples, using temperature-responsive polymers has emerged as a very promising avenue for

U. Gürer, O. Lieleg
Department of Materials Engineering
School of Engineering and Design
Technical University of Munich
Boltzmannstraße 15, 85748 Garching, Germany
E-mail: oliver.lieleg@tum.de

U. Gürer, O. Lieleg
Center for Protein Assemblies (CPA) and Munich Institute of Biomedical Engineering (MIBE)
Technical University of Munich
Ernst-Otto-Fischer Straße 8, 85748 Garching, Germany

F. von Usslar, C. Zollfrank
TUM Campus for Biotechnology and Sustainability
Technical University of Munich
Schulgasse 16, 94315 Straubing, Germany

 The ORCID identification number(s) for the author(s) of this article can be found under <https://doi.org/10.1002/admi.202300669>

© 2023 The Authors. Advanced Materials Interfaces published by Wiley-VCH GmbH. This is an open access article under the terms of the Creative Commons Attribution License, which permits use, distribution and reproduction in any medium, provided the original work is properly cited.

DOI: 10.1002/admi.202300669

controlling the properties of surfaces including their adhesiveness. For instance, by incorporating the synthetic macromolecule poly(N-isopropylacrylamide) (PNIPAM) into materials, it is possible to control their wettability, induce structural changes, and to change the adhesion behavior of the surface by altering the temperature level.^[20,21]

Of course, apart from choosing a dedicated component that responds to an external trigger in an adhesion system, a suitable matrix material needs to be selected first. Here, with (re-growable and thus easily available) wood still being its primary source, cellulose and its derivatives have emerged as a “green alternative” matrix for adhesives.^[22] For instance, Ferreira et al.^[23] presented an alkaline dispersion of cellulose fibrils for the bonding of paper, and this adhesive works in both, wet and dry conditions. Liu et al.^[24] developed a water-resistant wood adhesive by adding polyamines to dialdehyde cellulose. Furthermore, there are many different variants of cellulose with respect to form and size, which is why cellulose fibrils have gained considerable attention in material science. For instance, they show promising material enhancement properties, *inter alia*, regarding mechanical strength when used for 3D-printing,^[25] as a framework for transparent materials,^[26] and in biomineralized form, for example, as a network within amino clay adhesives.^[27]

In nature, cellulose is not only a main component of wood but also serves as the principal component in the structure of mucilaginous seeds, such as those from *Arabidopsis* and *Plantago ovata*, where a rigid cellulose fibril structure is surrounded by ductile polymers that are primarily composed of pectin macromolecules.^[28] Zhao et al.^[29] have found that the mucilage envelope of *Arabidopsis* seeds comprises two layers of mucilage: an adherent and a non-adherent one. The adherent mucilage envelope contains a significant amount of carbohydrates derived from hemicellulose and crystalline cellulose, whereas the non-adherent mucilage layer contains a much lower amount of crystallized cellulose. Mucilaginous seeds use their adhesion system to anchor themselves to the soil as required for successful germination. Thus, when transferring such a 3D adhesion system to a 2D surface, a fibrillar cellulose matrix is likely to be necessary.

Following these considerations, we here aim at creating a bio-inspired, tunable adhesion system by combining a biopolymer/cellulose framework inspired by mucilaginous seeds and a thermo-responsive polymer with adhesive properties. In a first step, to obtain a structural base matrix, we utilize readily available and cost-effective beech wood as the primary source of cellulose. In wood, the cellulose framework is embedded into a matrix of hemicelluloses and lignin.^[30] From this composite, we create a fibrillar surface canvas by applying a local delignification process, so the liberated cellulose fibers provide a high surface area while still being securely anchored to the intact wood matrix located below. In a second step, we attach pectin macromolecules to the cellulose layer by making use of the small helper molecule dopamine. With this two-component structure, we mimic the surface components and functional principle of mucilaginous seeds and provide macroscopic wood samples with adhesive properties. With the additional integration of PNIPAM polymers into this two-component structure, we can further tune the properties of the adhesion system by increasing its stickiness at elevated temperatures and rendering the detachment process

more compliant. Overall, our study pinpoints design strategies of how to tune the adhesion behavior of a surface by engineering the system on a molecular level.

2. Results and Discussion

To convert an intact wood matrix into a fibrillar surface, established delignification procedures^[31] need to be adjusted with regard to two aspects: process control and reaction conditions. Moreover, whereas there are well established techniques to fully^[32] and partially^[33] delignify wood specimen of different sizes, a locally controlled, partial delignification along the axial direction and on the axial surface of the sample has not been reported so far. Here, we design a tailored sample holder to ensure optimal local delignification and washing processes, to minimize handling efforts between distinct process steps and thus to protect the treated surface with its liberated fibrils in its fragile, wetted state. Additional requirements for this sample holder (Figure 1a; Figure S1, Supporting Information) include a good inertness with respect to the applied reaction chemicals used here (such as a sodium chlorite (NaClO₂) solution or hydrogen peroxide (H₂O₂) in an acidic environment), temperature resistance up to 90 °C, and reusability.

With a cylindrical shape of the wood specimen for subsequent adhesion measurements in mind, the custom sample holder is manufactured from silicone to keep the wood specimen floating on the surface of the delignification solution. This ensures that only one axial surface of the cylindrical wood sample is in contact during the reaction, while the major part of the wood matrix stays outside. Moreover, the sample holder is constructed to float on the solution when loaded with samples, and inserting the samples should tightly seal the cylindrical spaces thus preventing any reaction liquid from entering the sample holder. The latter is achieved by integrating a narrowed section into each cylindrical cavity of the holder, so that the silicone is strained by the wood specimen upon insertion, thus providing fixation and sealing simultaneously (Figure 1b). The circular shape of those openings ensures an even strain distribution around the sample and prevents the holder material from tearing apart. Since the whole construct is made from a single, flexible material, the sample holder is reusable, repairable and easy to clean. In such a customized sample holder, up to eight wood samples can be treated at the same time.

Still, when cylindrical wood samples are inserted into this sample holder to float on a delignification solution, another important issue must be considered: owing of the uniaxial tubular nature of the beech wood tissue, aqueous solutions are soaked irregularly into the wood structure by capillary forces. However, by adapting the viscosity and concentration of the delignification solution as well as the reaction time, we gain control over this issue and a locally restricted delignification process (Figure 1c,d; Figures S2 and S3, Supporting Information) can be achieved. For the NaClO₂ solution used here as a delignification agent, alginate is chosen as a viscosity increasing additive. The good stability of alginate under acidic conditions and elevated temperatures as well as its good solubility in water (as required for post reaction removal) were key properties for this choice.^[34]

To mimic the mucilaginous envelope, which comprises an ordered cellulose fibril layer in combination with a pectin coat,

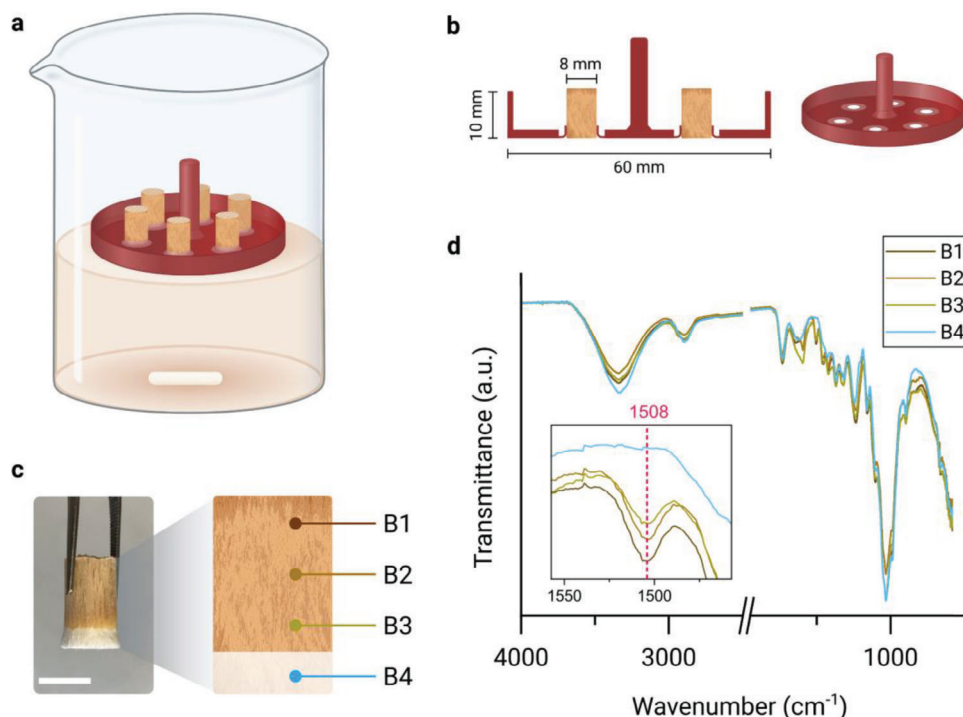


Figure 1. Overview of the partial delignification process. a) Illustration of the loaded sample holder as used during the delignification treatment. b) Shape and dimensions of the sample holder. c) Photograph of a partially delignified wood sample as obtained when using a NaClO_2 -solution for delignification treatment. The labelled spots along the longitudinal axis of the sample (B1-B4) indicate where the FTIR spectra shown in (d) were measured. The scale bar represents 8 mm. d) Spectra obtained from FTIR-ATR measurements: the aromatic vibrations of lignin at 1508 cm^{-1} are absent in the delignified region (B4).

the libriform fibers consisting of holocellulose on the surface of the beech wood sample are liberated by applying an adapted partial delignification process (Figure 2a, see Experimental section); in contrast, most previous studies utilize fully delignified wood, which comes at the price of high fragility unless further modified.^[35,36] SEM images show that the local delignification process applied indeed alters the surface morphology of the samples: Compared to the flat surface of untreated samples comprising fibrillar structures fixed in a dense matrix, delignified samples exhibit single liberated fibers (Figure 2b, Figures S4,S5, Supporting Information). In addition to this visual inspection of the delignified samples, a spectroscopic analysis of material collected from the sample surfaces confirms the success of the delignification treatment: In treated samples, the typical absorbance band of lignin at 280 nm is missing (Figure 2c). The same holds true for the aromatic vibration peak in FTIR at 1508 cm^{-1} . (Figure 1d)^[37,38]

In a second step of the wood modification process, a pectin layer is attached to the surface of the delignified wood samples by employing a dopamine-assisted coating process. Those pectin macromolecules are expected to act as load bearing anchors, and their firm attachment to the liberated cellulose fibers should be enabled very well by the intermediate layer of dopamine created during the coating process. Indeed, dopamine molecules can stably attach to a broad range of materials, which renders dopamine-based intermediate layers a versatile tool to generate macromolecular coatings.^[39–41] The FTIR spectra acquired from such modified surfaces confirm that this coating process was suc-

cessful. However, owing to the polysaccharidic nature of both cellulose and pectin, differences in the FTIR spectra are restricted to specific areas. The amine group from the dopamine (1616 cm^{-1}) broadens the band through N–H bending and antisymmetric stretching. Additionally, aromatic C–C stretching motions become visible (1520 cm^{-1}), as well as the C–H wagging vibration of the ring hydrogens of dopamine (800 cm^{-1}).^[42,43]

As expected, the FTIR signal originating from the pectin coating applied on top of the dopamine layer superimposes some of the dopamine-related characteristic modes, whereas the additional shoulder at 1048 cm^{-1} points toward additional C–O stretching vibrations. (Figure 2d). Furthermore, the vibration of –COOH groups of the pectin can be seen in the fingerprint region (830 cm^{-1}).^[45,46] Importantly, applying the dopamine-assisted pectin C coating maintains the increased surface roughness obtained by the delignification process (Figure 2e).

Having confirmed the successful attachment of a pectin coat to the delignified wood samples, adhesion tests are conducted on a glass surface (Figure 3a). For those tests, the treated surface of the samples is wetted, brought into contact with the glass surface, and kept in this contact for 20 min so the adhesion properties of the samples are probed in a moderately wet state. This particular contact time was selected as it returns consistent results with good adhesive properties whereas the samples are less sticky in their initial, fully wet state or when they approach a nearly dried state. A similar behavior can also be observed for the seeds of *Plantago lanceolata* and *Linum usitatissimum*, where their

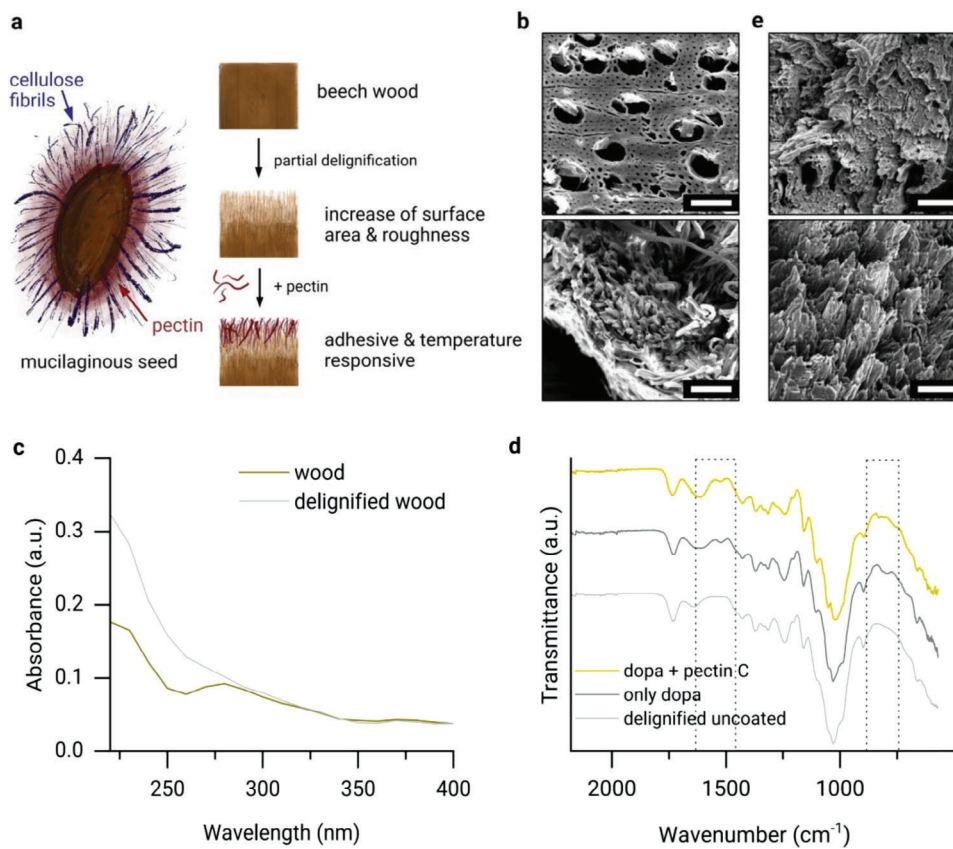


Figure 2. Envisioned strategy to create a bioinspired adhesive surface on beech wood. a) Schematic representation of a mucilaginous seed (adapted from ref. [44]) and of the treatment steps involved in creating an adhesive surface on a beech wood sample. b) SEM images comparing a non-delignified beech wood surface (top) to a peracetic acid (PAA) treated (and thus delignified) beech wood surface (bottom). Scale bars represent 90 μm . c) UV-vis absorbance spectra of beech wood (brown) as received and after delignification with PAA (gray). Data shown represents mean values as calculated from $n = 3$ independent samples. d) FTIR spectra of different PAA delignified beech wood surfaces: uncoated (gray), only dopamine coated (dark gray), and dopamine-assisted pectin C coated samples (yellow) are compared. e) SEM images of only pectin C coated (upper) and dopamine-assisted pectin C coated PAA delignified beech wood surface. The scale bar represents 90 μm .

stickiness decreases as the mucilage envelope of these seeds dries out.^[47]

For initial adhesion tests conducted with different delignified sample variants at room temperature, we observe the following: Without any coating or when carrying a dopamine coating only, the adhesiveness of the samples is very low with detachment stress values below $5.0 \times 10^{-3} \text{ N mm}^{-2}$ (Figure 3b). However, when the pectin layer is directly introduced onto the surface of the delignified samples (without using a dopamine pre-coating), we observe a small but significant increase in the mean detachment stress. Importantly, this effect becomes much more pronounced when the pectin layer is attached to the wood sample with the assistance of dopamine. On other surfaces (including tin coated steel, polystyrene, and flat beech wood), we also find adhesive properties for dopamine-assisted pectin C coatings generated on delignified beech wood samples – albeit with different detachment stress values than on glass (Figure S6, Supporting Information). Interestingly, when such a dopamine-assisted pectin C coating is applied to an undelignified wood sample, the recorded mean detachment stress is significantly lower. These results confirm that the dopamine-based intermediate layer promotes the attachment of pectin to the cellulose surface – most likely by a com-

bination of non-covalent and covalent bonds as brought about by the catechol groups present in the polydopamine layer.^[48] In detail, Hong et al.^[49] proposed that oxidation reactions of dopamine result in the formation of certain chemical structures, such as dopachrome and quinone, and these derivatives form compounds that are covalently bonded. Subsequently, these compounds physically attach to each other through weak interactions (van der Waals), cation- π interactions, and hydrogen bonds. Indeed, the adhesion propensity of existing catechols can even be improved: Very recently, synthetic non-canonical phenolic polymers were developed that contain 4–5 hydroxyl groups on an aromatic ring, resulting in a highly potent wet adhesive capable of reaching a lap-shear strength of up to 10 MPa.^[50]

The best adhesion results are obtained when topographical effects (as brought by delignification) and chemical effects (as brought by the pectin coating) are combined. Profilometric images obtained on samples agree with this hypothesis: the delignified samples exhibit a higher surface roughness (Figure 3c) than their undelignified counterparts, and applying the pectin coat even further increases the surface roughness. Our notion that the strength of the adhesion system depends on the surface roughness is further supported when analyzing samples that

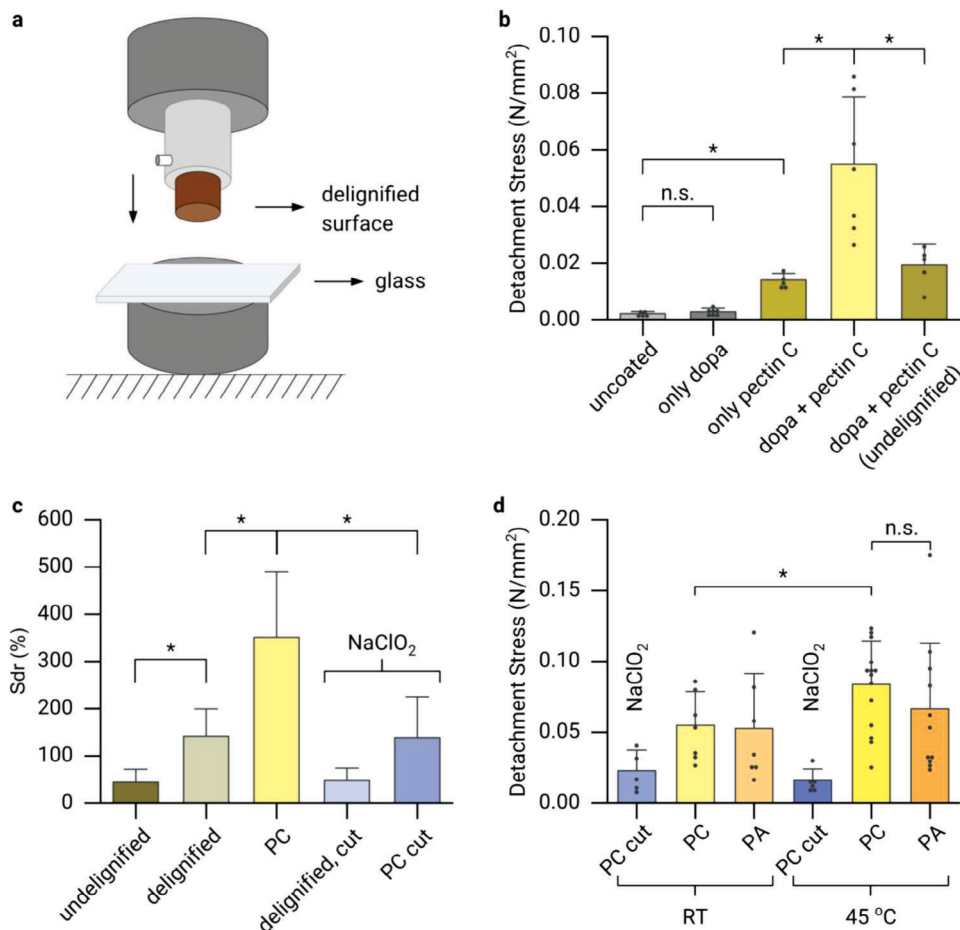


Figure 3. Detachment behavior and surface properties of different modified beech wood samples. a) Schematic illustration of the setup used for the adhesion tests. b) Detachment stress values obtained at RT for physically or chemically (dopamine-assisted) attached pectin C coatings on PAA delignified wood samples (surface area $\approx 30 \text{ mm}^2$) as well as for undelignified samples (surface area $\approx 50 \text{ mm}^2$). Data shown represents mean values, error bars depict the standard deviation as calculated from $n \geq 5$ independent samples. c) The developed interfacial area ratio (S_{dr}) is compared for different samples: undelignified (brown), PAA delignified (light brown), PAA delignified and dopamine-assisted pectin C coated (yellow), NaClO_2 delignified (light blue), and NaClO_2 delignified and dopamine-assisted pectin C coated (blue). Data shown represents mean values, error bars depict the standard deviation as calculated from $n \geq 15$ independent images. d) Adhesion behavior of differently coated wood samples (NaClO_2 delignified: blue; PAA delignified: yellow/orange): dopamine-assisted pectin C coating (PC) and pectin A coating (PA) at RT and $45 \text{ }^\circ\text{C}$. Data shown represents mean values, error bars depict the standard deviation as calculated from $n \geq 5$ independent samples. Asterisks and “n.s.” indicate statistically significant and non-significant differences, respectively (based on a p -value of 0.05).

were delignified with a different protocol (i.e., using NaClO_2 , see Experimental Section). Here, even with the dopamine-mediated pectin layer attached, the sample surface roughness is less than half of what we obtain with the other delignification protocol (Figure 3c) – and the same holds true for the corresponding detachment stress (Figure 3d). Moreover, when the surface roughness was increased via sandpaper treatment, the results demonstrate that liberating individual cellulose fibrils is crucial for increasing the adhesion properties of the surface: Upon applying a dopamine-assisted pectin C layer to those mechanically treated samples (where the surface roughness increased as well, see Figure S7, Supporting Information), we do not find increased adhesion compared to flat samples carrying the same coating (Figure S8, Supporting Information).

Of course, a successful delignification of the wood samples might also facilitate dopamine attachment to the sample by

rendering the hydroxyl groups on the cellulose and hemicelluloses more accessible. Indeed, it was suggested before that polydopamine can bind to cellulose via non-covalent interactions mediated by hydrogen bonds.^[51]

So far, we used a pectin variant found in citrus plants (pectin C); however, there are also other pectin variants, e.g., one found in apples (pectin A). When we modify the pectin C layer on the delignified wood samples with pectin A, we obtain very similar detachment stress values – at least at room temperature. However, plant seeds in nature are exposed to different temperature levels during spring and summer, so elevated temperatures might affect their adhesion properties. For instance, seeds from plants growing in warmer areas of the world tend to show a higher stickiness and a greater mucilage volume^[52,53]. Similarly, it appears possible that samples coated with pectin C and pectin A, respectively, differ in terms of their adhesion behavior at temperature levels above

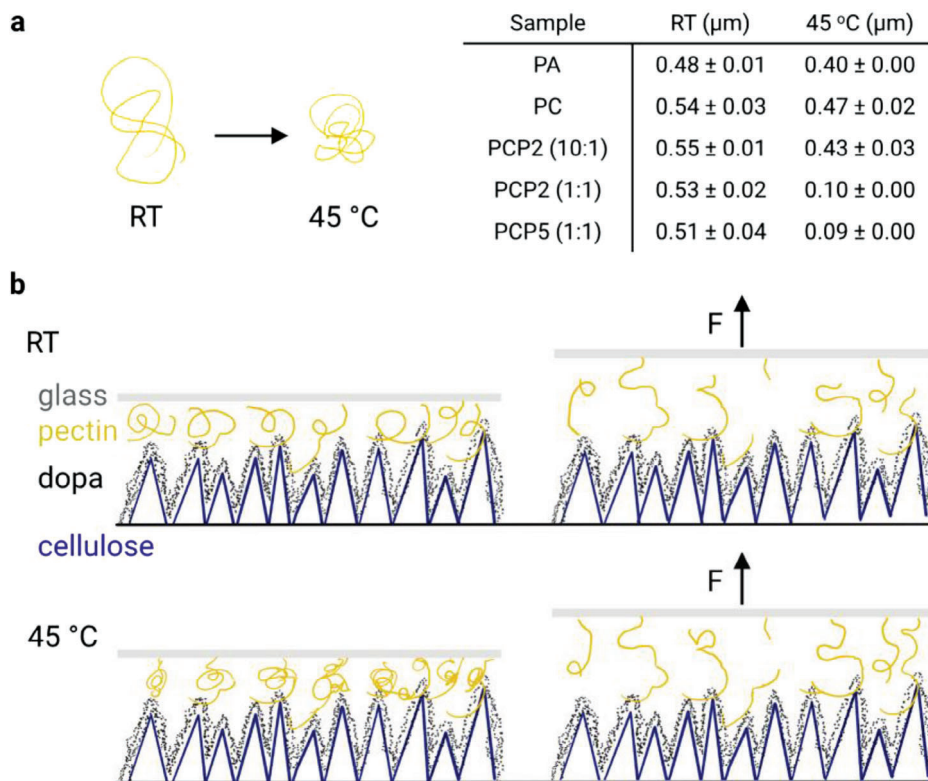


Figure 4. Temperature dependency of the hydrodynamic radii of pectins and pectin C/PNIPAM conjugates. a) Illustration of the temperature induced compaction of the macromolecules and hydrodynamic radii determined for the different constructs when analyzed as aqueous solutions reconstituted at 0.01% (w/v). Values shown represent averages together with the standard deviation as calculated from $n = 3$ independent samples. b) Schematic illustration depicting a putative explanation for the results obtained from the adhesion tests. When applying a normal force to the wood/glass interface, the pectin chains (yellow) that are attached to the rough, delignified wood surface (blue spikes) with the help of a polydopamine pre-coating (black dots) can be stretched before the two surfaces detach from each other. At the elevated temperature level of 45 °C, the pectin macromolecules (or pectin C/PNIPAM conjugates) are more strongly compacted, which allows for absorbing higher normal forces thus leading to higher detachment stresses and a more compliant interface.

RT. And indeed, we find an increase in the adhesion strength of both variants of pectin coated samples upon temperature increase (Figure 3d) – yet this effect is significant for pectin C.

Both pectin variants are long polysaccharide chains with short side chains, that is, flexible polymers whose conformation are largely dictated by entropic effects.^[54–56] Thus, at higher temperatures, such entropic effects will force the flexible polymer chains more strongly into a coiled-up, compacted conformation than at RT (Figure 4a). To ensure accurate size measurements on the two pectin variants, their concentration is reduced to 0.01% (w/v) (as higher concentrations often lead to increased turbidity of the solution arising from molecular aggregation effects). When we probe the hydrodynamic radii of the two pectin variants at RT using light scattering experiments, we find that pectin C is with $\approx 0.54 \mu\text{m}$ larger than pectin A ($\approx 0.48 \mu\text{m}$). Repeating those measurements at 45 °C, we find that the hydrodynamic radii of both pectin variants are decreased (i.e., by $\approx 13\%$ and $\approx 17\%$, respectively), which is in line with our expectation of entropy-driven compaction of the pectin structure and with findings reported in previous studies.^[57,58] In other words, at the elevated temperature level probed here, both pectin layers are present in a more condensed state than at RT. Thus, they can be expected to be further stretched (Figure 4b) in a detachment test conducted at 45 °C and

to absorb higher levels of normal forces before the samples detach. This might explain the increased detachment forces we find for pectin coated samples at 45 °C.

At this point, it is important to realize that pectin A and C differ in terms of their molecular structure. According to the literature, pectin A possesses a higher net charge, a more branched architecture and a higher molecular weight (M_n) than pectin C.^[59,60] These properties are also likely to explain why solutions reconstituted from pectin C exhibit a higher viscosity compared to pectin A solutions created at the same concentrations (Figure S9, Supporting Information). We speculate that, together, those differences in the molecule properties of the two pectin variants might be responsible for our observation that the detachment forces obtained for samples coated with pectin C are increased upon temperature more strongly than those obtained for samples coated with pectin A.

Having shown that the molecular configuration of the sticky pectin layer created on the surface of the delignified samples influences the behavior of the adhesive interface, we now ask if we can further tune the adhesion system developed here so it withstands higher detachment forces and becomes more compliant. To achieve this, we make use of an additional macromolecule, which has been shown to be very sensitive to

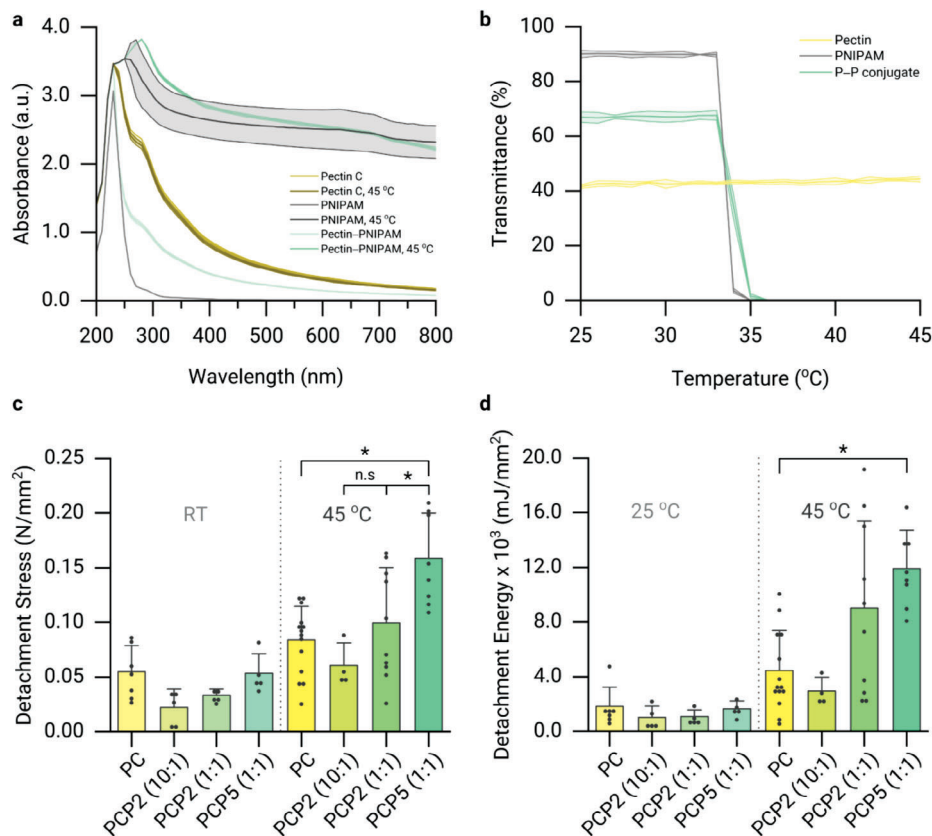


Figure 5. Characterization of pectin C/PNIPAM conjugates and of adhesive wood surfaces created therefrom. a) Absorbance and b) turbidity spectra of aqueous solutions of pectin C, PNIPAM (5.5 kDa), and their 1:1 (w/w) conjugate (concentration: 1.0% (w/v) each). Data shown represents mean values, error bars depict the standard deviation as calculated from $n = 3$ independent samples. c) Detachment stresses and d) detachment energies of wood samples carrying dopamine-assisted pectin C or pectin C/PNIPAM conjugate coatings; Results obtained at RT and at 45 °C are compared. Data shown represents mean values, error bars depict the standard deviation as calculated from $n \geq 4$ independent samples. Asterisks and "n.s." indicate statistically significant and non-significant differences, respectively (based on a p -value of 0.05).

temperature changes: PNIPAM^[61,62]. The idea is to create pectin C/PNIPAM conjugates, and that those conjugates should modify the adhesion strength and the plasticity of the detachment process.

Owing to key differences (e.g., functional groups) in the biochemical architecture of pectin C and PNIPAM, it should be possible to verify a successful conjugation of those two macromolecules by means of light absorption measurements. And indeed, pectin C chains exhibit a characteristic shoulder (Figure 5a) in the UV range (i.e., between 280 and 300 nm^[63,64]) whereas PNIPAM chains give rise to an absorbance peak at 229 nm, which originates from the C=O groups of this macromolecule.^[65] Moreover, the light absorption behavior of PNIPAM becomes stronger at 45 °C, which is the result of a transition from a loosely coiled molecule structure to a condensed globule entailing aggregation at this elevated temperature level.^[65,66] Importantly, such an increase in the absorption behavior is observed for the pectin C/PNIPAM conjugate, but not for unmodified pectin C (Figure 5a), which indicates that our conjugation attempt was indeed successful. Similarly, the turbidity of PNIPAM and pectin C/PNIPAM conjugate solutions increases at around 35 °C (Figure 5b) whereas the turbidity of an unmodified pectin solution remains unchanged, and NMR measurements

confirm the successful generation of a pectin C/PNIPAM conjugate (Figure S10, Supporting Information).

We conduct initial adhesion tests with a 10:1 conjugate created from pectin C and a 2.5 kDa variant of PNIPAM, and we refer to this construct as PCP2 (10:1). However, samples prepared with this conjugate demonstrate a similar performance (Figure 5c,d) as samples carrying a simple pectin C coating (PC) only – and this holds true at both, 25 and 45 °C.

Potentially, this unsatisfactory outcome may result from the low amount and small molecular weight (2.5 kDa) of PNIPAM present in the conjugate. Thus, we prepare additional pectin C/PNIPAM conjugates where we improve those two parameters. In the first variant, we increase the weight ratio of (2.5 kDa) PNIPAM to pectin C to 1:1 prior to conducting the coupling reaction. With this new PCP2 (1:1) conjugate, compared to samples carrying the PCP2 (10:1) construct, we find a slight (but not significant) increase in the mean detachment stress and detachment energy at 45 °C (Figure 5c,d). Moreover, for this new conjugate, an increase in temperature entails a noticeable increase in both, absorbance and turbidity, compared to PCP2 (10:1) (see Figure S11, Supporting Information). This suggests that, even though the changes in the adhesion properties detected so far were (owing to the heterogeneity of the obtained data) not significant, our

overall strategy is reasonable. Thus, we create another conjugate variant, where we employ a higher molecular weight version (5.5 kDa) of PNIPAM and mix it with pectin C in a 1:1 weight ratio when conducting the coupling step. When probed at 45 °C, samples coated with this PCP5 (1:1) conjugate now indeed show a significantly higher mean adhesion stress ($0.16 \text{ N} \times \text{mm}^{-2}$, Figure 5c) and detachment energy ($12.0 \times 10^{-3} \text{ mJ mm}^{-2}$, Figure 5d) than the PC group ($0.08 \text{ N} \times \text{mm}^{-2}$ / $4.5 \times 10^{-3} \text{ mJ mm}^{-2}$).

To rationalize these findings obtained from the detachment tests, we compare them to results from light scattering tests which report on the reduction of the hydrodynamic radii of the pectin C/PNIPAM conjugates upon temperature increase. Initially, both, unmodified pectin C and pectin C/PNIPAM conjugates exhibit comparable hydrodynamic radii at 25 °C (Figure 4a). When increasing the temperature to 45 °C, the different conjugates experience distinct levels of compaction: The PCP2 (10:1) conjugate, which contains a comparably low amount of the smaller PNIPAM (2.5 kDa) variant, shrinks by ~22%, whereas the unmodified pectin C shrinks by ~13 %. Here, it is important to note that the shrinkage result obtained for the conjugate represents an average value – but that we observed two peaks in the size spectrum recorded at 45 °C (Figure S12, Supporting Information). The latter suggests that, for this particular sample, two macromolecular variants coexist: pectin macromolecules attached to PNIPAM (2.5 kDa) and unconjugated pectin macromolecules. In other words, for the conditions chosen to create this conjugate, the amount of added PNIPAM was too low to obtain a high yield of conjugates – which is why the effect envisioned to be brought about by the PNIPAM component was too weak to dictate the adhesion behavior of the surface (and we observed similar values in the detachment stress and detachment energy as for unmodified pectin C).

However, when a tenfold higher amount of this PNIPAM (2.5 kDa) variant is employed to create the PCP2 (1:1) conjugate, the resulting construct exhibits both, a higher shrinkage rate of ~81% and a single peak in the size distribution obtained at 45 °C (Figure S12, Supporting Information). Still, the obtained size distribution is very broad with hydrodynamic radii ranging from 30 to 420 nm (Figure S12, Supporting Information). Accordingly, for the macroscopic adhesion behavior of samples created with this PCP2 (1:1) conjugate, we do observe an increase in the detachment stress and detachment energy – but the high sample-to-sample variants (resulting from the molecular heterogeneity of the created conjugate) prevent those differences from being significant (Figure 5d).

In contrast, when the larger PNIPAM (5.5 kDa) variant is utilized to create the final PCP5 (1:1) conjugate, we find both, a strong reduction in size upon temperature increase (i.e., by ~82%, Figure 4a) and a narrower size distribution (Figure S12, Supporting Information). Consequently, the samples created from PCP5 (1:1) show a significant increase in both, the detachment stress and detachment energy compared to samples coated with unmodified PC as well as better reproducibility compared to samples coated with other conjugates. Thus, together with the results obtained from the spectroscopic analysis of the different conjugates, our results agree with the literature that, when a pectin/PNIPAM conjugation is prepared, the amount and molecular weight of the chosen PNIPAM variant are both cru-

cial to control the solubility of the construct and the temperature-induced compaction of the molecule.^[67,68]

Overall, in our detachment tests, we observed a heterogeneous failure behavior among the samples – even within a specific group. Regardless of the sample group, there were occasions where we observed the presence of residual pectin on the glass surface following the detachment of the sample. Conversely, there were tests where no such residues were detected. Therefore, for our system, a combination of both, adhesive and cohesive failure, seems to be relevant. If cohesive failure occurs, it may take place at different locations of the functionalized wood sample: at the cellulose-dopamine interface, at the dopamine-pectin (or dopamine-pectin/PNIPAM conjugate) interface, or between distinct pectin (or pectin C/PNIPAM) molecules. However, rheological measurements and quartz crystal microbalance with dissipation monitoring (QCM-D) tests (Figure S13, Supporting Information) suggest that the last option is less likely as we do not find indications for strong pectin-pectin (or conjugate-conjugate) interactions.

3. Conclusion

Here, we introduce a complex surface structure that draws inspiration from a natural adhesion system. By partially mimicking the intricate architecture of mucilaginous envelopes, we engineer adhesive surfaces that can operate in a wet state. In a bottom-up approach, we combine the cellulose fibrils liberated from a wood matrix with a hybrid macromolecule that unites the flexible polysaccharide pectin with the thermo-responsive polymer PNIPAM and thus obtain control over the strength and compliance of the adhesive system. To optimize the system introduced here, further improvements to the wood matrix could be pursued to achieve even better adhesion properties. For instance, additionally employing an enzymatic delignification route to enhance the delignification efficiency^[69] could potentially lead to an even higher surface roughness. Alternatively, replacing the pectin used here with a different adhesion-conveying chemical component may be another strategy to improve properties of the system. Indeed, a similar strategy employing a chitosan/PNIPAM conjugate has also shown promising results for the development of bio-based wet adhesives for medical applications.^[70]

4. Experimental Section

Sample Holder Preparation: The sample holder was manufactured from two-component silicone rubber (1:1 w/w, TFC Silikon Kautschuk Typ 3 HB), Troll Factory, Riede, Germany) by pouring it into a glass petri dish, carefully wetting the whole inner surface. Custom circular molds made from the lid of sample capsules (polypropylene, \varnothing 11 mm, BEEM) were added, dipping only two thirds into the base layer of the silicone, evenly distributed across the plane in the same number as samples were required. After curing for 2 h, a second layer of silicone rubber was applied to the inner walls of the mold and the center handle made from the same material was added. The sample holder was demolded after 24 h of curing. Following the removal of the small spacer molds, the middle of each recess was cut with a hole punch (4 mm in diameter).

Sample Preparation: Extraction and delignification: Before applying the delignification protocol, beech wood samples were prepared using a Soxhlet extraction method. In brief, the Soxhlet extractor was filled with beech

wood samples cut into cylinders with a diameter of 8 mm (radial tangential plane) and a length (longitudinal) of 10 mm. Two extraction rounds were conducted, each lasting 8 h. Initially, an extraction was carried out at 115 °C using a 1:0.25 (v/v) mixture of acetone ($\geq 99.5\%$, Carl Roth, Karlsruhe, Germany) and distilled water. The second extraction was performed by using 150 mL of toluene ($\geq 99.5\%$, Carl Roth) at 140 °C. Subsequently, the extracted samples were cleaned with an 80% (v/v) ethanol solution and left to air-dry overnight at room temperature. Selected samples (NaClO₂ route) were cut axially using a microtome (Reichert-Jung Ultracut E) to even the surface before applying the delignification process.

For the delignification step, a peracetic acid solution (PAA) was prepared by mixing 100 mL of hydrogen peroxide (H₂O₂, 35%, pure, stabilized, Carl Roth) and 100 mL of acetic acid (100%, Carl Roth) under continuous stirring, following an adapted previously reported protocol.^[32] The extracted samples were fixed to the sample holder which floated on the surface of the PAA solution; the floating samples were incubated at 90 °C for 5 h. Once the sample surfaces facing the PAA solution turned completely white, any remaining acid and residues were washed off by sample incubation in 2 L of distilled water overnight. Finally, the washed samples were air-dried at room temperature.

In a second delignification method, sodium alginate (1.0 % (w/v), very low viscosity, Thermo Fisher Scientific, Waltham, USA) was slowly added to a solution of sodium chlorite (10% (w/v), AppliChem, Darmstadt, Germany) until fully dissolved. After heating to 80 °C, the floating sample holder was placed on the surface of this solution, and the reaction was started by adding 4.0% (w/v) glacial acetic acid (100% purity, VWR). After 4 h, the samples were rinsed and washed overnight on 1 L of distilled water. This procedure was repeated once, until the surface facing the solution showed no remaining coloration (Figure S5, Supporting Information). Then, the samples were frozen in liquid nitrogen and subsequently lyophilized (−45 °C, 0.095 mbar, Christ Alpha 2–4 LDplus, Christ, Osterode, Germany) for 6 h.

Pectin/poly(N-isopropylacrylamide) conjugation: To functionalize pectin C (Carl Roth) chains, carbodiimide-induced cross-linking was used. In brief, 1 g of pectin C (Carl Roth) was dissolved in 80 mL of 2-(N-morpholino)ethanesulfonic acid buffer (MES, 10×10^{-3} M, pH = 5). Then, 50 mg of 1-ethyl-3-(3-dimethylaminopropyl) carbodiimide hydrochloride (EDC, Carl Roth) and 50 mg of N-hydroxysulfosuccinimide sodium salt (NHS, 98% purity, abcr GmbH, Karlsruhe, Germany) were added. After 3 h of incubation, the solution was mixed with a Poly(N-isopropylacrylamide) (PNIPAM, amine terminated, $M_n = 2.5$ kDa, Sigma-Aldrich) solution (1 g dissolved in 20 mL of MES, 10×10^{-3} M, pH = 5). The mixture was incubated overnight under a fume hood and then dialyzed (MWCO = 12–14 kDa, Spectra/Por) against distilled water at room temperature for 2 days. The dialyzed solution was freeze-dried for 3 days and rehydrated directly before further use. The same procedure was used to functionalize pectin C with another PNIPAM variant (amine terminated, $M_n = 5.5$ kDa, Sigma-Aldrich). PCP2 (10:1), PCP2 (1:1), and PCP5 (1:1) were abbreviations for dopamine-assisted pectin C conjugate coatings generated on PAA delignified surfaces. PCP2 (10:1) and PCP2 (1:1) refer to conjugates created by using initial weight ratios between pectin C and 2.5 kDa PNIPAM of 10:1 and 1:1, respectively. Similarly, PCP5 (1:1) represented a conjugate formed using an initial weight ratio of 1:1 between pectin C and 5.5 kDa PNIPAM.

Dopamine-assisted pectin coating: To generate a pectin (or conjugate) coating on the surface of the delignified samples, a previously reported protocol was followed with slight changes.^[71] In brief, dopamine hydrochloride (Sigma-Aldrich, St. Louis, MI, USA) was dissolved to a concentration of 0.4% (w/v) in TRIS buffer (50×10^{-3} M, pH = 8.5). By employing the sample holder described above, the delignified samples were placed onto this solution for 1 h and 30 min. Afterward, the samples were washed with distilled water and immediately placed onto a solution containing 4.0 % (w/v) pectin (or a pectin-PNIPAM conjugate) dissolved in distilled water for 1 h. Finally, the coated samples were air-dried at room temperature. In the results section, the abbreviations PC and PA refer to dopamine-assisted coatings carrying pectin C and pectin A, respectively.

Physico-Chemical Analyses: **SEM:** Samples were carefully cut from the delignified surface of the specimens, mounted with double-sided carbon pads and sputter-coated (Pt/Au, 90 s at 40 mA, Bal-Tec SCD 050, Balzers, Liechtenstein). Unless stated otherwise, pictures were acquired at 30.0 kV (DSM 940 A, Zeiss, Germany).

Topographical characterization: To quantitatively assess the surface topography of the samples, profilometric images were captured using a laser scanning microscope (VK-X1000 series, Keyence Corporation, Osaka, Japan) equipped with a 20X lens. A minimum of 15 images were taken for each sample, and the acquired topographical data was subsequently evaluated and processed using the software MultiFileAnalyzer (Keyence Corporation) to eliminate distortions arising from sample tilt. Subsequently, the metrological parameter S_{dr} (the developed interfacial area ratio) was calculated based on the processed data.

Spectroscopy: UV–vis absorbance spectra of different materials were performed using a microplate reader (SpectraMax ABS Plus, Molecular Devices, San Jose, USA). To conduct the analysis of beech wood and PAA delignified beech wood samples, particles were scraped from their surfaces, and the obtained material was suspended in distilled water to a concentration of 0.1% (w/v); then, UV–vis absorbance spectra (from 220 to 450 nm) were recorded at 25 °C. Pectin and pectin conjugates were dissolved to a concentration of 1.0% (w/v) in distilled water, and UV–vis absorbance spectra (from 200 to 800 nm) were recorded at both 25 and 45 °C. The turbidity and hydrodynamic radius (calculated from Stokes–Einstein equation) of aqueous solutions containing 1.0% (w/v) and 0.01% (w/v) of either conjugate, respectively, were determined using a particle size analyzer (Litesizer 500, Anton Paar, Graz, Austria) over a temperature range of 25 and 45 °C.

FTIR-ATR measurements were conducted on dried samples to evaluate the progress of delignification and to detect the coatings with 16 scans at a resolution of 2 cm^{-1} ($500\text{--}4000 \text{ cm}^{-1}$, Frontier, Perkin Elmer, Waltham, USA).

Adhesion Tests: The adhesion properties of different wood samples were evaluated using a commercial research grade shear rheometer (MCR 302, Anton Paar, Graz Austria). Prior to conducting the adhesion tests, the delignified surface of each sample was immersed in distilled water for 2 min. Then, the sample was fixed into a custom-made sample holder that was mounted into the upper grip of the rheometer using an adapter (D-CP/PP 7, Anton Paar). A commercial glass slide was fixed to the bottom plate (P-PTD 200, Anton Paar) of the rheometer to serve as a counter surface for the adhesion tests. To initiate the test, the upper grip was gradually lowered toward the glass slide until a normal force of 1.5 N (resulting in a zero gap) was detected. After a contact time of 20 min, the measurement head of the rheometer was lifted up at a constant speed of $10 \mu\text{m s}^{-1}$ until the sample was fully removed from the glass surface and the resulting force versus distance data was recorded. From those curves, the detachment stress and the detachment energy were calculated by taking into account the surface area of each sample. For adhesion tests conducted above room temperature, the temperature of both, the water used to wet the sample surface and the control unit of the rheometer, was set to 45 °C.

Statistical analysis: To conduct statistical analyses, the software OriginLab (Northampton, Massachusetts, USA) was used. Initially, a Shapiro–Wilk test was conducted to confirm the normal distribution of the measured values. Then, a two sample Student's *t*-test was employed to normally distributed populations with similar variances whereas a two-tailed Welch's *t*-test was utilized in cases where the variances were unequal. In such cases, where the data was not normally distributed (e.g., for the S_{dr} values of undelignified samples and for the adhesion tests of PA at 45 °C) a Mann–Whitney test was applied. In all cases, a *p*-value of $p \leq 0.05$ (corresponding to a confidence level of 95%) was chosen as a threshold for significance; significant differences were marked with an asterisk.

Supporting Information

Supporting Information is available from the Wiley Online Library or from the author.

Acknowledgements

U.G. and F.U. contributed equally to this study. The authors thank Stanislav Gorb, Clemens Schaber, and Helen Gorges for helpful discussions. This work was supported by a grant from the German Research Foundation (DFG Nr. 447247094) award to O.L. and C.Z.

Open access funding enabled and organized by Projekt DEAL.

Conflict of Interest

The authors declare no conflict of interest.

Data Availability Statement

The data that support the findings of this study are available from the corresponding author upon reasonable request.

Keywords

cellulose, partial delignification, pectin, wood

Received: August 11, 2023

Revised: October 17, 2023

Published online: November 28, 2023

- [1] T.-P. Huynh, Y. Chen, F. L. Bach-Gansmo, J. Dehli, V. N. Ibsen, M. Foss, A. S. Tvilum, A. N. Zelikin, H. Birkedal, *Adv. Mater. Interfaces* **2023**, *10*, 2201491.
- [2] M. Kim, J. Park, K. M. Lee, E. Shin, S. Park, J. Lee, C. Lim, S. K. Kwak, D. W. Lee, B.-S. Kim, *J. Am. Chem. Soc.* **2022**, *144*, 6261.
- [3] L. P. Bré, Y. Zheng, A. P. Pêgo, W. Wang, *Biomater. Sci.* **2013**, *1*, 239.
- [4] G. Meloni, O. Tricinci, A. Degl'innocenti, B. Mazzolai, *Sci. Rep.* **2020**, *10*, 15480.
- [5] Z. Xu, Z. Liu, C. Zhang, D. Xu, *J. Appl. Polym. Sci.* **2022**, *139*, e52894.
- [6] B. K. Ahn, *J. Am. Chem. Soc.* **2017**, *139*, 10166.
- [7] S. Erramilli, J. Genzer, *Soft Matter* **2019**, *15*, 4045.
- [8] J. M. R. Bullock, W. Federle, *Insect Sci.* **2011**, *18*, 298.
- [9] W. Federle, D. Labonte, *Philos. Trans. R. Soc. Lond., B, Biol. Sci.* **2019**, *374*, 20190199.
- [10] A. F. Galloway, P. Knox, K. Krause, *New Phytol.* **2020**, *225*, 1461.
- [11] W. Wei, J. Yu, C. Broomell, J. N. Israelachvili, J. H. Waite, *J. Am. Chem. Soc.* **2013**, *135*, 377.
- [12] C. Cui, W. Liu, *Prog. Polym. Sci.* **2021**, *116*, 101388.
- [13] I. S. Bayer, *Adv. Mater. Interfaces* **2022**, *9*, 2200211.
- [14] C. Cai, Z. Chen, Y. Chen, H. Li, Z. Yang, H. Liu, *J. Polym. Sci.* **2021**, *59*, 2911.
- [15] H. Lee, B. P. Lee, P. B. Messersmith, *Nature* **2007**, *448*, 338.
- [16] Y. Zhou, M. Chen, Q. Ban, Z. Zhang, S. Shuang, K. Koynov, H.-J. Butt, J. Kong, S. Wu, *ACS Macro Lett.* **2019**, *8*, 968.
- [17] T. Nakamura, Y. Takashima, A. Hashidzume, H. Yamaguchi, A. Harada, *Nat. Commun.* **2014**, *5*, 4622.
- [18] S. Reddy, E. Arzt, A. Del Campo, *Adv. Mater.* **2007**, *19*, 3833.
- [19] H. Kim, K. Kim, S. J. Lee, *NPG Asia Mater* **2017**, *9*, e445.
- [20] M. Dompé, M. Vahdati, F. Van Ligten, F. J. Cedano-Serrano, D. Hourdet, C. Creton, M. Zanetti, P. Bracco, J. Van Der Gucht, T. Kodger, M. Kamperman, *ACS Appl. Polym. Mater.* **2020**, *2*, 1722.
- [21] W. Song, H. Li, C. Wang, B. Yang, *Adv. Mater. Interfaces* **2014**, *1*, 1400009.
- [22] H. Zhang, P. Liu, S. M. Musa, C. Mai, K. Zhang, *ACS Sustainable Chem. Eng.* **2019**, *7*, 10452.
- [23] E. S. Ferreira, E. M. Lanzoni, C. A. R. Costa, C. Deneke, J. S. Bernardes, F. Galembeck, *ACS Appl. Mater. Interfaces* **2015**, *7*, 18750.
- [24] S. Liu, G. Du, H. Yang, H. Su, X. Ran, J. Li, L. Zhang, W. Gao, L. Yang, *ACS Sustainable Chem. Eng.* **2021**, *9*, 16849.
- [25] M. Latif, Y. Jiang, B. Kumar, J. M. Song, H. C. Cho, J. Kim, *Adv. Mater. Interfaces* **2022**, *9*, 2200280.
- [26] T. Benselfelt, M. Nordenström, S. B. Lindström, L. Wågberg, *Adv. Mater. Interfaces* **2019**, *6*, 1900333.
- [27] K. Li, S. Jin, X. Li, J. Li, S. Q. Shi, J. Li, *J. Chem. Eng.* **2021**, *421*, 129820.
- [28] J. L. Phan, J. M. Cowley, K. A. Neumann, L. Herliana, L. A. O'donovan, R. A. Burton, *Sci. Rep.* **2020**, *10*, 11766.
- [29] X. Zhao, L. Qiao, A.-M. Wu, *Sci. Rep.* **2017**, *7*, 40672.
- [30] P. Fratzl, R. Weinkamer, *Prog. Mater. Sci.* **2007**, *52*, 1263.
- [31] M. Jakob, A. R. Mahendran, W. Gindl-Altmutter, P. Bliem, J. Konnerth, U. Müller, S. Veigel, *Prog. Mater. Sci.* **2022**, *125*, 100916.
- [32] M. Frey, D. Widner, J. S. Segmehl, K. Casdorff, T. Keplinger, I. Burgert, *ACS Appl. Mater. Interfaces* **2018**, *10*, 5030.
- [33] A. Kumar, T. Jyske, M. Petric, *Adv. Sustain. Syst.* **2021**, *5*, 2000251.
- [34] S. Thakur, B. Sharma, A. Verma, J. Chaudhary, S. Tamulevicius, V. K. Thakur, *J. Clean. Prod.* **2018**, *198*, 143.
- [35] M. Zhu, J. Song, T. Li, A. Gong, Y. Wang, J. Dai, Y. Yao, W. Luo, D. Henderson, L. Hu, *Adv. Mater.* **2016**, *28*, 5181.
- [36] P. Grönquist, M. Frey, T. Keplinger, I. Burgert, *ACS Omega* **2019**, *4*, 12425.
- [37] B. George, E. Suttie, A. Merlin, X. Deglise, *Polym. Degrad. Stab.* **2005**, *88*, 268.
- [38] T.-C. Chang, H.-T. Chang, C.-L. Wu, S.-T. Chang, *Polym. Degrad. Stab.* **2010**, *95*, 516.
- [39] C. Kimna, B. Winkeljann, J. Song, O. Lieleg, *Adv. Mater. Interfaces* **2020**, *7*, 2000735.
- [40] B. Miller Naranjo, S. Naicker, O. Lieleg, *Adv. Mater. Interfaces* **2023**, *10*, 2201757.
- [41] M. G. Bauer, O. Lieleg, *Macromol. Mater. Eng.* **2023**, *308*, 2200681.
- [42] A. Ghanbari, F. Warchomicka, C. Sommitsch, A. Zamanian, *Coatings* **2019**, *9*, 584.
- [43] A. Thakur, S. Ranote, D. Kumar, K. K. Bhardwaj, R. Gupta, G. S. Chauhan, *ACS Omega* **2018**, *3*, 7925.
- [44] A. Kreitschitz, E. Haase, S. N. Gorb, *Sci. Nat.* **2021**, *108*, 2.
- [45] A. Koziol, K. Sroda-Pomianek, A. Górniak, A. Wikiera, K. Cyprych, M. Malik, *Coatings* **2022**, *12*, 546.
- [46] E. A. M. S. Almeida, S. P. Facchi, A. F. Martins, S. Nocchi, I. T. A. Schuquel, C. V. Nakamura, A. F. Rubira, E. C. Muniz, *Carbohydr. Polym.* **2015**, *115*, 139.
- [47] A. Kreitschitz, A. Kovalev, S. N. Gorb, *J. Nanotechnol.* **2016**, *7*, 1918.
- [48] T. M. Lutz, C. Kimna, A. Casini, O. Lieleg, *Mater. Today Bio* **2022**, *13*, 100203.
- [49] S. Hong, Y. Wang, S. Y. Park, H. Lee, *Sci. Adv.* **2018**, *4*, eaat7457.
- [50] B. Cheng, J. Yu, T. Arisawa, K. Hayashi, J. J. Richardson, Y. Shibuta, H. Ejima, *Nat. Commun.* **2022**, *13*, 1892.
- [51] Y. Xie, Y. Zheng, J. Fan, Y. Wang, L. Yue, N. Zhang, *ACS Appl. Mater. Interfaces* **2018**, *10*, 22692.
- [52] E. F. Lopresti, M. E. Stessman, S. E. Warren, K. Toll, *J. Ecol.* **2023**, *111*, 525.
- [53] V. S. Pan, M. McMunn, R. Karban, J. Goidell, M. G. Weber, E. F. LoPresti, *Funct. Ecol.* **2021**, *111*, 525.
- [54] P. Nelson, C. Marshall, *Biol. Phys.: Energy, Inf., Life* **2008**, *Updated First Edition*, 342.
- [55] C. Bouchiat, M. D. Wang, J.-F. Allemand, T. Strick, S. M. Block, V. Croquette, *Biophys. J.* **1999**, *76*, 409.
- [56] C. Ortiz, G. Hadziioannou, *Macromolecules* **1999**, *32*, 780.
- [57] M. A. Masuelli, *Int. J. Biol. Macromol.* **2011**, *48*, 286.
- [58] A. M. F. Lima, V. Soldi, R. Borsali, R. Borsali, *J. Braz. Chem. Soc.* **2009**, *20*, 1705.

- [59] X. Ma, W. Chen, T. Yan, D. Wang, F. Hou, S. Miao, D. Liu, *Food Chem.* **2020**, *309*, 125501.
- [60] H. Kastner, U. Einhorn-Stoll, B. Senge, *Food Hydrocoll* **2012**, *27*, 42.
- [61] K. Nagase, *Adv. Colloid Interface Sci.* **2021**, *295*, 102487.
- [62] C. Wu, X. Wang, *Phys. Rev. Lett.* **1998**, *80*, 4092.
- [63] D. J. Messenger, A. R. Mcleod, S. C. Fry, *Plant Cell Environ* **2009**, *32*, 1.
- [64] S. Shankar, N. Tanomrod, S. Rawdkuen, J.-W. Rhim, *Int. J. Biol. Macromol.* **2016**, *92*, 842.
- [65] S. Makharza, J. Auisa, S. A. Sharkh, J. Ghabboun, M. Faroun, H. Dweik, W. Sultan, M. Sowwan, *Int. J. Polym. Anal.* **2010**, *15*, 254.
- [66] A. Murugadoss, A. Khan, A. Chattopadhyay, *J. Nanopart. Res.* **2010**, *12*, 1331.
- [67] K. Nagase, M. Watanabe, A. Kikuchi, M. Yamato, T. Okano, *Macromol. Biosci.* **2010**, *11*, 400.
- [68] K. Nagase, S. Ishii, K. Ikeda, S. Yamada, D. Ichikawa, A. M. Akimoto, Y. Hattori, H. Kanazawa, *Sci. Rep.* **2020**, *10*, 11896.
- [69] M. Moniruzzaman, T. Ono, *Biochem. Eng. J.* **2012**, *60*, 156.
- [70] R. Xu, S. Ma, Y. Wu, H. Lee, F. Zhou, W. Liu, *Biomater. Sci.* **2019**, *7*, 3599.
- [71] J. Song, T. M. Lutz, N. Lang, O. Lieleg, *Adv. Healthcare Mater.* **2021**, *10*, 2000831.